Design and Implementation of PV based Energy Harvester for WSN Node with MAIC algorithm

Hemalatha RAJENDRAN, Ramaprabha RAMABADRAN, Radha SANKARARAJAN
SSN College of Engineering, Chennai-603110
hemalathar@ssn.edu.in

***Abstract*—Wireless sensor networks (WSNs) are hardly in need of an additional source of power other than the normally used batteries, to increase the lifetime considerably. In this paper, mathematical modeling of photovoltaic energy harvesting (PVEH) system for the WSN is presented. The system comprises of the solar PV panel, boost converter as maximum power point tracker with moving averaged incremental conductance (MAIC) maximum power point (MPP) algorithm, Ni-MH battery for energy storage, compensator, buck regulator and the mathematically modeled WSN mote. MAIC algorithm is proposed to avoid the effect of drastic variations in input irradiance, in locking the MPP point. WSN mote is modeled in both active and sleep state based on the power consumption. To maintain the voltage stability, proper compensator has been designed for the proposed system. The performance of the system is tested for dynamic variations of environmental conditions using MATLAB simulation. The proposed system has 50 to 60 percent improved conversion efficiency when compared to the conventional direct coupling method. The parameters of the photovoltaic panel model have been validated through experimentation. Also the practical verification of the operation of MPPT circuit has been performed.**

***Index Terms*—DC-DC power converters, energy harvesting photovoltaic cells, solar energy, wireless sensor networks.**

I. Introduction

WSN consists of spatially distributed autonomous sensors to monitor physical or environmental conditions, such as temperature, sound, vibration, pressure, motion or pollutants. The development of WSN was motivated by military applications such as battlefield surveillance; today such networks are used in many industrial and consumer applications. WSN is suited for long lived applications, deployed in wide area at large densities. But the life time of the network is limited since it has battery as the energy resource. It is also hard to replace or recharge nodes battery once they are deployed. To achieve longer operational lifetime of batteries energy harvesting can be used. Solar energy is an attractive solution to increase the autonomy of the sensor networks to achieve perpetual operation [1]. The power conversion efficiency of the photovoltaic (PV) panel is rather low and it has nonlinear voltage-current (V-I) characteristics. This nonlinearity is due to temperature or irradiance level change in the environment which introduces variation in the MPP of the PV panel. Therefore it is essential to use maximum power point tracker (MPPT) to adjust the operating point of the solar panel and get the maximum output power from the PV panel in an efficient way. Battery is used as the storage element to store the energy available and to supply the load power during the period without solar power or when there is any shortage in power. Nowadays small solar panels suffice to ensure continued operation and a large number of PV harvesting circuits [2]-[8] have been proposed recently. A low power MPPT using the adaptive MPP tracking algorithm suitable for WSN node is developed in [2]. They used current mode control and achieved power conversion efficiency in the range of 50%-60%. DuraCap [3], a solar-powered energy harvesting system used supercapacitor and lithium-ion batteries for energy storage. It also uses pulse frequency modulation (PFM) based regulator switching for multiple MPPT operation. Batteryless solar-harvesting circuit [4] is also proposed for the low power applications but it is difficult to power the mote in cloudy and bad weather conditions. Ambimax [5] does MPP tracking autonomously and charges supercapacitors at maximum efficiency. It uses 70 mAh Li-Polymer battery and two 10 F super capacitors as energy storage elements. It also utilizes multiple energy harvesting sources such as solar, wind, thermal, and vibration. Prometheus [6] used a MOS switch with simple DC/DC converter for power conversion. Harvested energy is stored in two stage energy storage consisting of two super capacitors in series and rechargeable lithium battery (200 mAh**)**. In PV charger system [7] with SEPIC converter, peak current mode control is used with the batteries as the storage element. The elements of the harvesting circuit are decided based on the solar panel and the battery used. An energy harvesting circuit fabricated using a 0.35-μm CMOS process is proposed in [8]**.** MPPT circuit used exploits a successive approximation register and a counter to solve the tradeoff problem between a fast transient response and a small steady-state oscillation with low-power consumption. This paper considers the simple method of harvesting, for the chosen PV panel and the battery. Boost converter is chosen for its reliable operation at varying conditions.

Many MPPT control techniques have been proposed in the last decades [9]-[18]. The algorithms that are frequently used are Perturb and Observe algorithm [9], Incremental conductance algorithm [10], Constant voltage control [11], Constant current control [11], Pilot cell and artificial intelligent method using Fuzzy logic control [12] and neural network controller [13]. An in depth survey of all possible MPPT techniques available in the literature is presented in [14]-[16]. An intelligent control method for MPPT using the fuzzy logic control is proposed in [17]. The system performance is tested under varying irradiance and temperature conditions by MATLAB simulation. A variable step size incremental MPPT to provide better dynamic response and to achieve wide operating range is

Digital Object Identifier 10.4316/AECE.2015.02014

presented in [18].

Based on the literature survey it is observed that the PV fed power conditioning circuits (PCC) have been developed and different voltage ranges have been obtained, which is suitable to power up the WSN mote. There is a lagging part for the proper modeling of WSN mote for different states of WSN. It is felt that the proper modeling of the mote will be helpful to study the real time characteristics of the PV based WSN mote system. Hence in this paper the efforts have been made for the modeling of WSN mote under two major states viz. Active and Sleep. The interface of this model with PCC gives the realistic characteristics of the PV harvester system.

As complicate MPP algorithms consume much power in WSN platform MAIC algorithm with voltage mode controller is used in this paper. Moreover, type III compensation has been designed to ensure the stable operation of the PVEH system. The functioning of the proposed system has been validated through MATLAB/SIMULINK and results are presented for different system variations. The developed model for the mote has been checked via experimentation.

This paper is organized as follows: Section 2 discusses the PVEH system in detail, Section 3 gives the details of the load modeling, Section 4 deals the compensator design for the boost converter, Section 5 discusses the simulation of the PVEH system with simulation results and conclusions are presented in Section 6.

II. PV Energy Harvesting System

The proposed simple PVEH system is shown in Fig. 1. It consists of the mote that is modeled mathematically as the load, based on its power requirement.

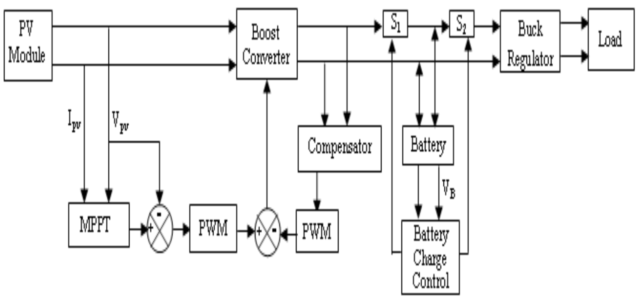

Figure 1. Block diagram of the proposed PV energy harvesting system.

The energy generated by the solar PV panel is efficiently stored in the battery with the boost converter and the MPPT in action. The duty cycle of the converter is varied by direct control based on the output from the MPPT. Compensator circuit is included to ensure stability in the system. Battery supplies power to the load, to get the voltage level (2.7 V - 3.3 V) sufficient for the mote, buck regulator is used. Battery charge control is included to avoid over charging and draining of the battery.

A. PV panel Modeling

The Blue Solar SL8585mm PV panel is used for the MATLAB simulation model. The panel provides 950 mW of nominal maximum power. It is of monocrystalline type and it is well suited with the requirement range of WSN. Datasheet values at standard test conditions (STC) of the cell are listed in Appendix A.

The simple one diode model [19] is used for modeling the PV panel in simulation. The voltage-current and voltage-power characteristics of the PV panel at T = 25 ºC and varying irradiance levels are shown in Fig. 2.

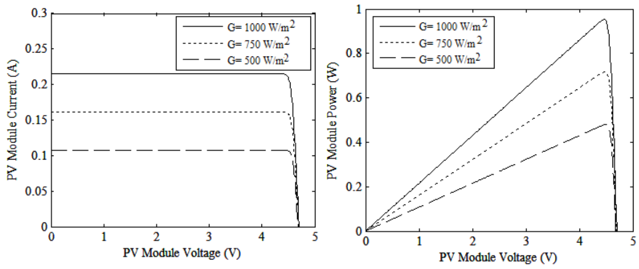

Figure 2. Simulated characteristics of the PV panel at T=25ºC

The irradiance change introduces a considerable change in the peak power, whereas the change in temperature does not produce a drastic variation in the peak power. More over in Indian scenario the temperature profile during a day does not experience a wide variation, excluding the exceptions on a few rare occasions. Hence the temperature is kept constant for further analysis.

B. Design of MPPT

In this paper, boost converter is used as MPPT. The converter is chosen based on the required battery voltage (4.8 V-5.6 V) and the available PV voltage level (V_m = 4.5 V). The voltage ratio of the boost converter is given as,

$$\frac{V_{in}}{V_o} = \left(1 - D\right) \tag{1}$$

$$\Delta I = \frac{V_{in} D}{fL} \tag{2}$$

$$\Delta V_c = \frac{I_o D}{fC} \tag{3}$$

where ΔI , ΔV_c is the ripple current and ripple voltage, D is the duty cycle of the converter, V_{in} is the input voltage of boost converter and V_o is the output voltage of boost converter. The inductor and capacitor values are designed by considering that the converter operates in continuous conduction mode (CCM). The values of L and C are calculated with voltage and current ripple of 5% based on (2) and (3). The ripple percentage is selected 5% because the life time of the PV panel will be reduced with higher ripple current at the input side. Moreover, the ripple percentage is calculated with respect to the expected steady state DC component. The obtained values are $L \geq 107$ mH and $C \geq 123.29$ μF with switching frequency, f_s = 10 kHz. Hence to ensure CCM L=200 mH and C=200 μF have been used in simulation.

B. Maximum Power Point Tracking Algorithm

The maximum power extracted from the PV panel depends mainly on three factors: irradiance level, load impedance and panel temperature. When the PV panel is directly connected to the load, the system will operate at the intersection of the V-I curve and load characteristics, which can be far from the MPP. MPP will vary dynamically based on the irradiance level and temperature. The MPP production is therefore based on the load characteristics adjustment under varying atmospheric conditions. PVEH system should be designed to operate at the maximum output power levels for any temperature and solar irradiation levels at all times. Hence the MPPT controller is used to match the source resistance to load resistance as seen by the PV panel (source) to extract maximum power. The duty cycle is set to its optimal value corresponding to the optimal operating point (V_m, I_m) using MPPT.

A simple MAIC algorithm has been proposed in this paper as shown in Fig.3. When there is a sudden change in the environment or the climatic condition around the PVEH system over a short duration of time, there is a chance of erroneous result in the MPP. To overcome this a third order moving average filter is included. It calculates the average of consecutive three samples of current and voltage of the PV panel. The moving averages are used to calculate the differential voltage and current values, from which the conductance value will be calculated and based on that the panel voltage, will be either increased or decreased. In this work marginal error (E) of 0.002 is included. Panel voltage will determine the duty cycle of the converter.

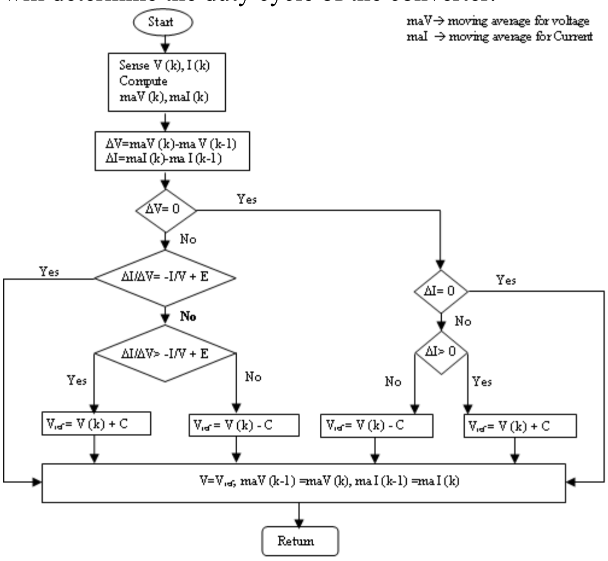

Figure 3. Incremental conductance algorithm over the moving averaged input

Moving average filter is implemented in recursive fashion using (4) and (5) as it has faster implementation, reduced complexity (one addition and one subtraction after the calculation of the first average) and integer based implementation. The values of p and q are taken as 1 and 2 respectively.

$$maV(i) = maV(i-1) + V(i+p) - V(i-q) \tag{4}$$

$$maI(i) = maI(i-1) + I(i+p) - I(i-q) \tag{5}$$

The input and output power of the MPPT system are simulated under varying irradiance levels G=500 W/m^2 and G=1000 W/m^2 are shown in Fig. 4 (a) and Fig. 4 (b).

The irradiance level changes after 0.5 s. It is observed that the MPPT tracks the maximum power in 0.12 s in the simulation and the changes are tracked properly, the input and output power remains the same approximately. As the boost converter is used, the output current is less than that of the input current and the output voltage is higher than that of the input voltage which is depicted in the Fig. 4 (c), (d), (e), and (f) respectively, but output power is equal to input power excluding the system losses. It is observed that the system loss is around 50 mW. The operation of the MPPT system has been checked for other irradiance levels too.

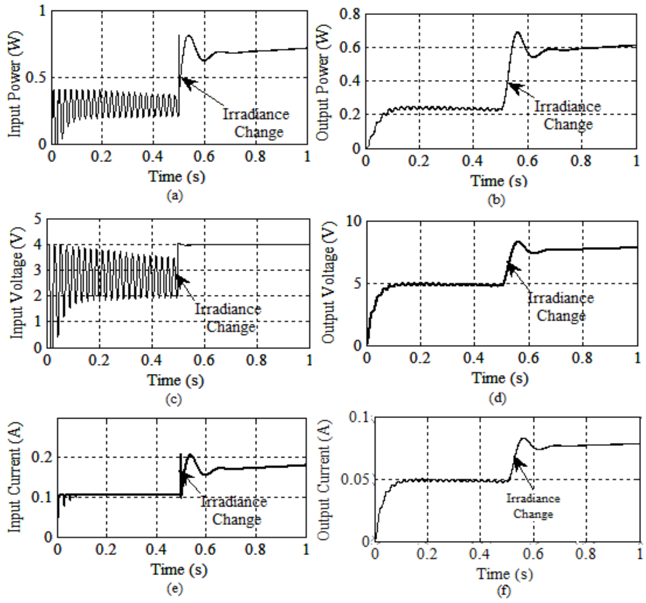

Figure 4. (a), (b) Input and output power of the MPPT system, (c), (d) Input and output current of the MPPT system, (e), (f) Input and output voltage of the MPPT system

B. Battery with Controller

In this paper NiMH battery is chosen considering the advantages like: better performance, long battery life, extremely low battery cost, stable performance due to flat discharge curve, no memory effect, easy charging and usage. 4.8 V, 150 mAh Nickel metal hydride (NiMH) rechargeable battery is used in the proposed system and the specifications are given in Appendix A.

Dynamic modeling of the battery is performed in MATLAB with (6) and (7) by considering both the charging and discharging states [20].

$$V_{batt} = -R \times i - K \times \frac{Q}{Q - it} \times \left(it + i^*\right) + Exp(t) \tag{6}$$

$$V_{batt} = E_o - R \times i - K \times \frac{Q}{|it| - 0.1 \times Q} \times i^* - K \times \frac{Q}{Q - it} \times i + Exp(t) \tag{7}$$

where V_{batt} is the battery voltage (V), E_o is the battery voltage (V), K is the polarisation resistance (Ω), Q is the battery capacity (Ah), 'it' is the actual battery charge (Ah) and i^* is the filtered current (A).

The battery used has a nominal voltage of 4.8 V and fully charged voltage of 5.62 V. The battery state of charge is controlled with two switches and a charge control algorithm providing series charge regulation of the PVEH system. Whenever the battery terminal voltage is higher than the upper limit of the charging cycle (80% State of Charge) the switch S_1 in Fig. 1 is opened and prevents the overcharging of the battery and increases its lifetime. If the battery voltage is less than the lower critical limit (20% State of Charge) and there is no power available from the solar panel the switch S_2 in Fig. 1 is opened to avoid the deep discharge of the battery.

As the battery full charge voltage is 5.62 V, to make it suitable for the operating range of the mote (2.7 V-3.3 V) step down converter is used after the battery. The duty cycle of the buck converter is adjusted using the voltage mode controller to set the output voltage to approximately 2.7 V. The output voltage can also be fixed at any range between (2.7 V-3.3 V)

III. MODELING OF WSN MOTE

The power consumption of the WSN mote depends mainly on the duty cycle (D_1) of mote, active mode current (I_{active}) and sleep mode current (I_{sleep}) which is decided based on the application. The average power consumption P_{avg} of the mote is given by

$$P_{avg} = V_{supply} \times \left(D_1 \times I_{active} + \left(1 - D_1\right) \times I_{sleep}\right) \quad (8)$$

where V_{supply} is the input voltage supplied to the mote. The active and sleep state energy consumption is modeled based on its current consumption and voltage of operation. For this work Mica2 mote is considered. The current consumption of the mote in active and sleep states is taken from the datasheet as shown in Table I and the power consumption is calculated.

TABLE I. MOTE CURRENT CONSUMPTION

Mica2, MPR400CB, ATMEGA 128	Processor State		Radio State		
	Active	Sleep	Transmit	Receive	Sleep
Current Consumption	8 mA	<15 µA	27 mA	10 mA	<1µA

The current consumption of the Mica2 mote in sleep state is less than 16 µA and the active state is 35 mA. The supply and voltage range of the mote is 2.7 V to 3.3 V. The simple relation between power, voltage and resistance is given by (9).

$$R = \frac{V^2}{P} \quad (9)$$

Using (9) and the data listed in Table I the mote is modeled as resistor depending on its power consumption and the corresponding values are calculated and listed in Table II.

TABLE II. MOTE-RESISTANCE MODELING

Mote Name	Power Consumption		Load Resistance	
	Active (mW)	Sleep (µW)	Active (Ω)	Sleep (kΩ)
Mica2, MPR400CB, ATMEGA 128	95	44	76.73	165.68

The schematic representation of this model is shown in Fig. 5. The model of the mote has two resistors in parallel; one represents mote in active state and the other represents the mote in sleep state. These parallel resistors are controlled by a switch in series having the input as the step response based on the duty cycle (D_1) of the mote.

For the time T_1= (D_1 × period of simulation), active state resistor is included and for the remaining time T_2= ((1-D_1) × period of simulation), sleep state resistor is included in the system. The choice of the resistor (active or sleep) is made by the step response given.

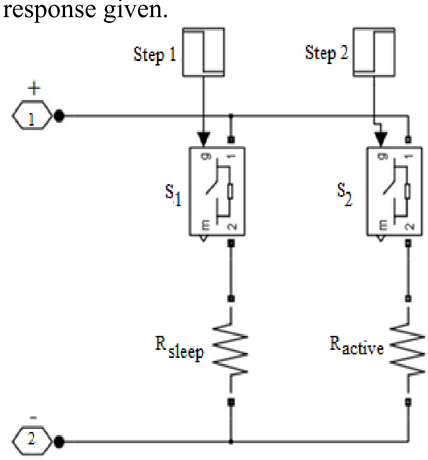

Figure 5. Schematic of the modeled load

IV. COMPENSATOR DESIGN

The stability of the PVEH system is ensured with the proper design of the compensator circuit in the model. This section describes the method to evaluate the compensator parameters based on the converter topology used. The stability analysis has been carried out with the transfer function model of the elements in the system.

The small signal model of the boost converter in continuous conduction mode (CCM) is obtained by the averaged modeling. The high-frequency switching ripples in the inductor current and capacitor voltage waveforms are removed by averaging over one switching period. An averaged small signal ac equivalent circuit of the boost converter is considered and the battery is modeled as capacitor and included before the load. The control to output transfer function of the boost converter with battery is derived as below,

$$TF_{vd}(s) = \frac{G_{do}\left(1 - \frac{s}{\varpi_z}\right)}{1 + \frac{s}{Q\varpi_o} + \left(\frac{s}{\varpi_o}\right)^2} \quad (10)$$

where the parameter values are dc gain G_{do}=V/D', angular frequency of zero $\varpi_z = D'^2 R/L$, angular corner frequency $\varpi_z = D'\sqrt{L(C0 + C1)}$ and the quality factor Q=R $D'\sqrt{(C0 + C1)}/\sqrt{L}$. From the converter transfer function it is evident that it has a right half plane zero (RHPZ) which will lead to instability of the system. The boost transfer function and the compensator design is made for the irradiance levels of 1000 W/m^2 and 300 W/m^2. Critical value of the L and C is considered in both the extreme irradiance levels.

Design of the compensator circuit around the voltage mode control is easier under light load conditions, as the WSN scenario is of light load condition, Type III compensator is chosen here. Compensator is added to get minimum error in the voltage loop and to move the right half plane zero into the stability region [21]. The transfer function of the compensator is given by,

$$TF_{Type\,III} = \frac{R_1+R_3}{R_1C_1R_3}\left(\frac{\left(s+\frac{1}{R_zC_z}\right)\left(s+\frac{1}{\left(R_1+R_3\right)C_3}\right)}{\left(s+\frac{\left(C_1+C_z\right)}{R_zC_1C_z}\right)\left(s+\frac{1}{R_3C_3}\right)}\right) \tag{11}$$

The procedure used for the design of the compensator is as follows: i) value of f_0 and f_z are calculated ii) output capacitance (C) value of the boost converter is altered to satisfy the condition $f_0 \leq 0.1\ f_{RHP}$ and the obtained frequency is considered as f_{LC} , iii) Crossover frequency is placed at $f_c \leq .33\ f_z / f_{RHP}$ iv) change in phase is reduced by placing the zeros at 70% of f_{LC} , v) gain = compensation gain – 20 log (modified f_z / f_c), vi) 20 log(R_2 / R_1) = gain and vii) R_1 R_2 R_3 C_1 C_2 C_3 are calculated using the following relations $1/2\pi R_2C_2=0.7f_{LC}$, $1/2\pi R_1C_3=0.7f_{LC}$, $1/2\pi R_2C_1=0.7f_Z$ and $1/2\pi R_3C_3=0.7f_Z$. The final gain is calculated using (11). The compensator element values obtained by using the above design equations for the proposed system are R_1=100 kΩ, R_2=25.93 kΩ, R_3=6.98 kΩ, C_1=59.03 nF, C_2=844.8 nF and C_3=19.06 nF. The bode diagram of the compensated boost is as shown in Fig. 6.

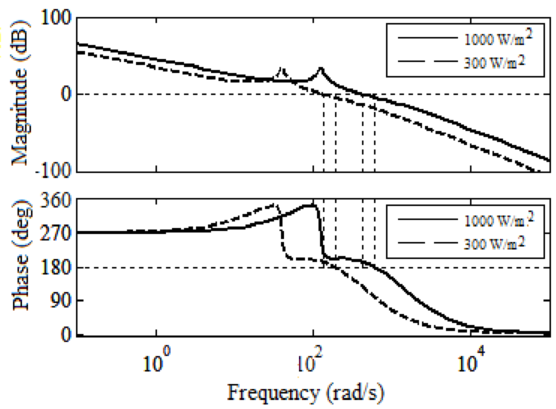

Figure 6. Bode plot of the compensated boost converter in open loop

It has a phase margin and gain margin as 4.16 dB and 13.8 ° at 1000 W/m^2, 3.995 dB and 13.13 ° at 300 W/m^2. Thus the converter is made stable by moving the RHPZ into the stable region.

V. Results and Discussion

The simulation schematic of the entire PVEH system is shown in Fig. 7.

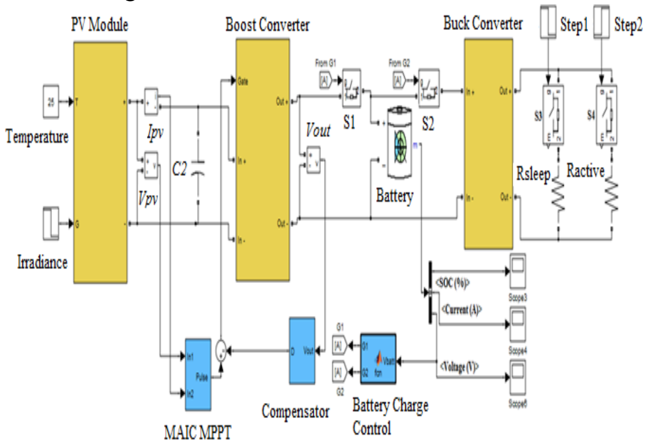

Figure 7. Schematic of the PVEH system

The PVEH system has been tested with Mica2 as the mote of interest under two different scenarios. In the first test scenario the irradiance level (G) is kept as 1000 W/m^2 and the temperature (T) is taken as 25 ºC for the entire simulation duration. Mote is assumed to be in sleep state for the first half of the duration and in active state for the next half duration. Initial state of charge of the battery is taken as 50%. Second test scenario has the parameters as G=500 W/m^2 for the first 0.5 s and G=1000 W/m^2 during the next 0.5 s, T=25 ºC and the mote state is assumed to have a duty cycle of 1% as most of the WSN applications have a duty cycle < 1 %.

Under these test conditions the input and output power of the converter is observed and shown in Fig. 8. The output tracks the corresponding changes in the input, the output and the input power are approximately same due to the usage of MAIC algorithm.

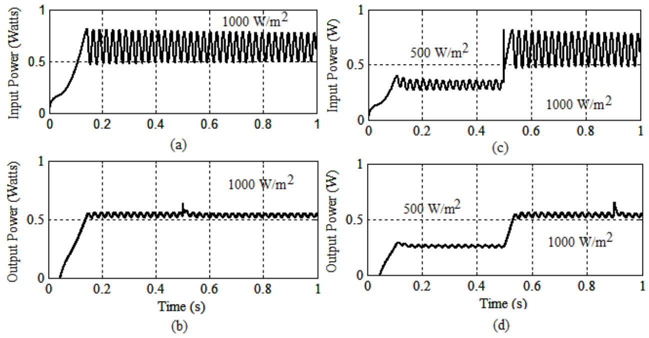

Figure 8. Input and output power of the converter for the different test scenarios

During the initial 0.5 s the mote is in sleep state and it consumes nearly (43~45) µW. During the last 0.5 s the mote is in active state and it consumes nearly 95~98 mW. Similarly the mote current consumption in sleep state is nearly 16 µA and during active state it consumes nearly 33~36 mA. The power consumption of the mote is as shown in the Fig. 9. The mote power consumption also varies according to the change in the duty cycle.

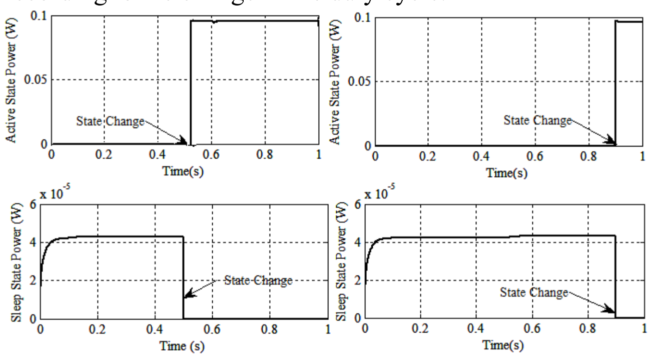

Figure 9. Power consumption of the mote

The battery State of Charge (SOC) in both scenarios is shown in Fig. 10.

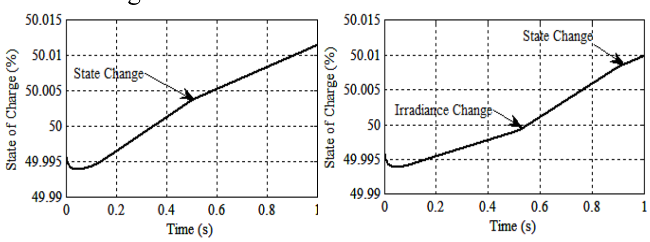

Figure 10. State of charge of the battery

It shows that the linear increase in SOC till 0.5 s, then as the mote becomes active, current consumption increases and the battery current reduces accordingly hence, the rate of change in SOC decreases after 0.5 s. In Fig. 10 (b) SOC increases linearly upto 0.5 s, at 0.5 s irradiance level change occurs so the current entering the battery is increased hence, the rate of increase of SOC also increases. After 0.9 s the mote becomes active so the rate of increase in the SOC decreases. The corresponding change in the battery current is shown in Fig. 11.

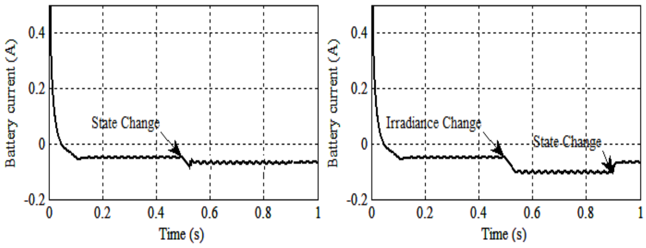

Figure 11. Battery current

The comparison of the output power obtained, with the conventional direct coupling method [17] and the PVEH method is carried out and the results are shown in Fig. 12.

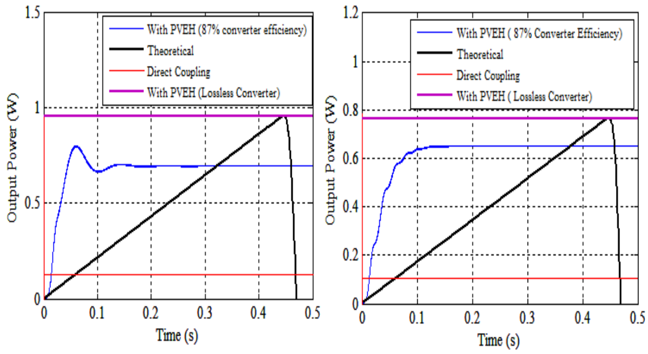

Figure 12. Comparative analysis of the output maximum power harvested at 1000 W/m2, 25 ºC and 800 W/m2, 20 ºC.

The analysis is carried out under different illumination and temperature conditions. The results shown are for the irradiance levels 1000 W/m^2 and 800 W/m^2 at 25 ºC and 20 ºC respectively. Direct coupling of the mote with solar panel yields very less amount of power conversion due to impedance mismatch. Proposed PVEH produces 85% of the theoretical maximum power with 87% efficiency converter on an average. PVEH has better energy conversion efficiency under varying irradiance and temperature too.

The designed compensator discussed in section 4 has been incorporated in closed loop of PVEH system and analyzed for stability. The transfer function of the elements in the loop is given in (12), where $TF_{vd}(s)$ is calculated using (10) and G_{pwm} is the gain associated with the PWM modulator. The gain of PWM modulator is given by $1/V_M$, where V_M is the maximum voltage range considered for the reference signal used in PWM. The transfer function of the entire feedback loop is given in (13).

$$T(s) = TF_{vd}(s) \times TF_{Type\ III} \times G_{pwm} \tag{12}$$

$$VL(s) = T(s) \big/ \left(1 + T(s)\right) \tag{13}$$

The bode diagram of the loop including the pulse width modulator is as shown in Fig. 13 for different irradiance levels. It has phase and gain margins as 29.9 dB, and 46.83 ° at 1000 W/m^2, 29.74 dB and 47.04 ° at 300 W/m^2. Thus the system is in stable state at the extreme cases of irradiance level change.

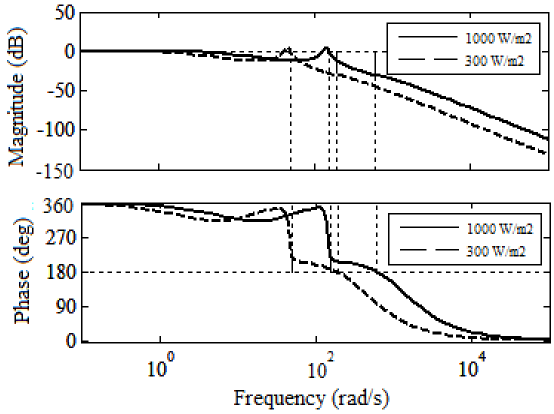

Figure 13. Bode plot of the voltage loop

The step response of the voltage loop is as shown in Fig. 14. The system settles at 0.505 s with the irradiance level of 1000 W/m^2 and it takes 1.67 s to settle down with the irradiance level of 300 W/m^2 indicating the difficulty in achieving faster stable state in low irradiance levels. The system stability in the intermediate irradiance levels are also checked and found to be stable.

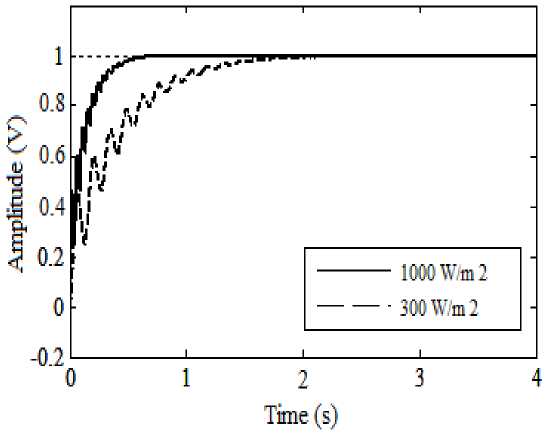

Figure 14. Step response of the voltage loop

A. Experimental Validation

The proposed system has been modeled and simulated in the previous section, the proper functioning of the system is proved extensively through the simulation results. The functioning of the proposed MAIC MPP and PV panel are verified experimentally.

The parameter variations for other than the test conditions given by the manufacturer (Appendix A) have been evaluated through experimental characteristics using electronic load method [22]. To realize the electronic load, MOSFET IRF7101 (with ratings of 20 V, 3.5 A, 0.10 Ω) is used. The entire electronic setup used to measure the I-V characteristics of the PV panel is shown in Fig. 15. The characteristic displayed is for the irradiance level of 700 W/m^2. The major PV model parameters like diode ideality factor and series resistance have been evaluated. Based on the observations and calculations, series resistance of 443 mΩ and diode ideality factor of 1.1 is used to make the simulation model more realistic.

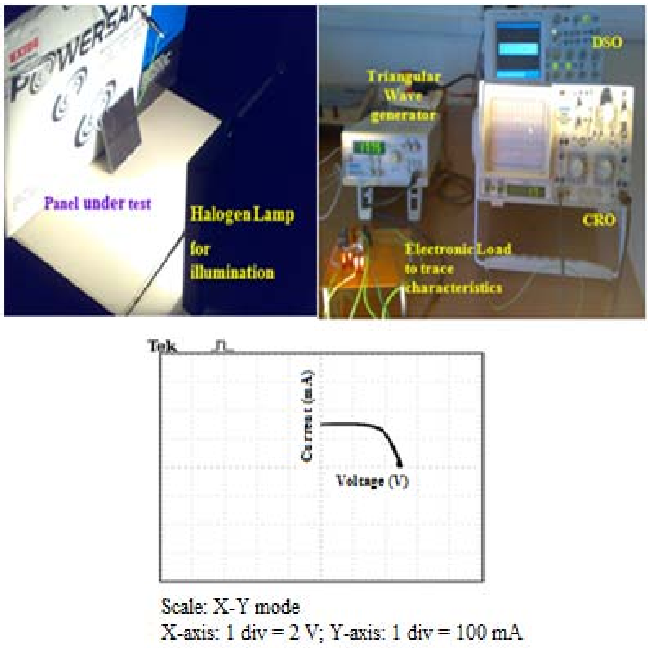

Figure 15. Experimental verification of the PV panel characteristics

The hardware realization of the MPPT system has been performed. The components/devices used are IRF 7101, ZLLS410, PLA10AN3030R4R2 (90 mH) and CKR capacitors. PIC16F877A microcontroller is used to implement the MAIC algorithm. The experimental setup and the results are presented in Fig. 16.

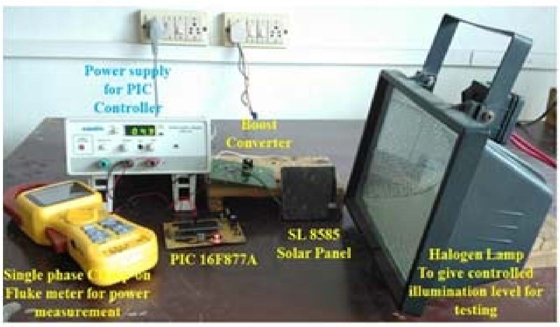

a)

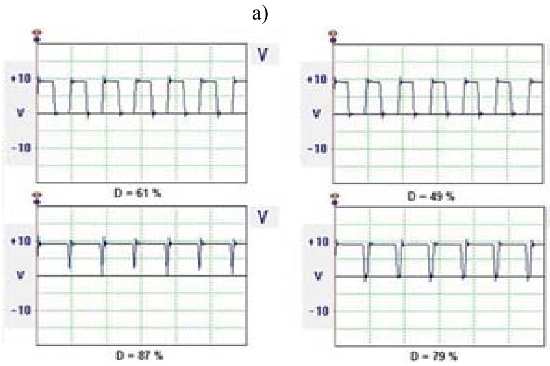

b)

Figure 16. (a) Experimental setup for MPPT circuit, (b) Gate pulse waveforms for different irradiance levels

The capability and operation of the MAIC algorithm has been experimentally verified by varying irradiance on the panel using halogen lamp. It is observed that the algorithm varies the pulse width to track the maximum power. These variations are shown in Fig. 16 (b). It is observed that, when irradiance changes, duty cycle is also changed to vary the equivalent load resistance seen by the source to track maximum power. The input and output power observed is shown for irradiance level of 484 W/m^2 in Fig. 17. The results are observed using single phase clamp on fluke meter to read the power directly. The measured values of V_{oc}, I_{sc} are 5.42 V and 104 mA respectively. The expected maximum power is 410 mW.

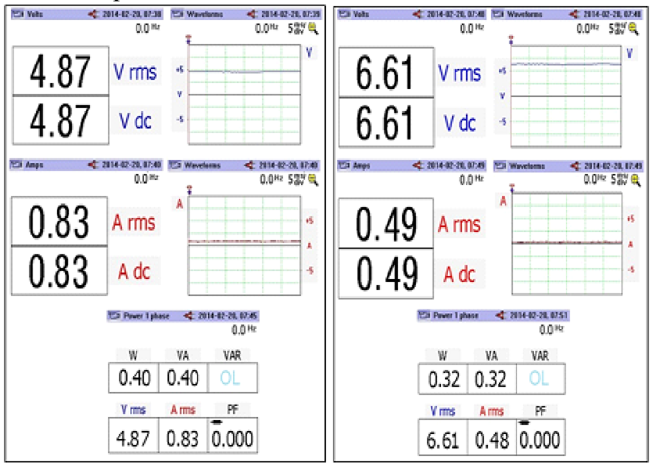

Figure. 17. Input and output voltage, current and power measurements for irradiance level 484 W/m2

From Fig. 17 it is observed that the power at the source side is 400 mW and at the output is 320 mW. The system losses are 80 mW whereas for the same condition the system losses in simulation are around 50 mW. The power for different irradiance levels have been observed experimentally in the same way. It is found that the average efficiency of the MPPT system is 85 % and the observed practical losses are deviated (about 35 %) from that of the simulation results. The reduction in power loss, thereby increase in efficiency can be further enhanced by proper fabrication of the MPPT converter with hermetical sealing.

VI. Conclusion

In this paper, PVEH system with the simple mote model is presented. The mote has been modeled as two resistors, which correspond to wake and sleep modes of the mote. The modeling has been performed based on the real time power consumption of the mote on both the modes. The proposed PVEH system enables the testing of the harvester under varying load conditions and the different states of the mote. The different parts of the proposed system have been designed and modeled using MATLAB. The MAIC MPPT is used to remove the effect of sudden irradiance change on the choice of MPP. Simulations have been carried out by having the mote state in 1 % duty cycle which coincides with the real time requirement of the WSN. The stability in the system is also ensured by proper implementation of compensator circuit. The results validate the proper operation of the system under varying irradiance levels and different load states.

Operation of the PV panel and the MPPT algorithm is also validated experimentally. The energy production from the PVEH will increase the stand by energy available in the WSN mote. Proposed PVEH will increase the lifetime of the mote and avoid the necessity of replacing or recharging the batteries. Thus the PVEH system can be used for the WSN motes to enhance their lifetime from the abundantly available renewable energy. The hardware implementation of the entire harvester will be accomplished in future to evaluate its functioning in real time environment. The ripples at the PV panel parameters can be minimized with interleaving principles. The MEMS based realization and single chip implementations of the PVEH system are the possible extensions of the work in future.

Appendix A

PV Panel: Maximum Power-P_{max}=950 mW, Voltage at maximum power-V_m=4.5V, Current at maximum power-I_m=210 mA, Open circuit Voltage-V_{oc}=4.7V, Short circuit Current-I_{sc}=215 mA, Temperature coefficient of Power= - 0.47% / °C, Temperature coefficient of I_m= + 0.1%/°C, Temperature coefficient of V_m= - 0.38% / °C.

Battery: Nominal Voltage = 4.8 V, Nominal Capacity = 110 mAh, Typical Capacity = 120 mAh, Internal Resistance = 1 Ω.

References

[1] A. Hande, T. Polk, W. Walker, D. Bhatia, "Indoor solar energy harvesting for sensor network router nodes," J. Microprocessors & Microsystems, vol. 31, no.6, pp.420-432, 2007. [Online]. Available: http://dx.doi.org/10.1016/j.micpro.2007.02.006

[2] C. Alippi, C. Galperti, "An adaptive system for optimal solar energy harvesting in wireless sensor network nodes," IEEE Trans Circ Syst, vol.55, no.6, pp. 1742-1750, 2008. [Online]. Available: http://dx.doi.org/2008. 10.1109/TCSI.2008.922023

[3] C. Y. Chen, P. H. Chou, "Duracap: a supercapacitor-based, power-bootstrapping, maximum power point tracking energy-harvesting system," in *Proc. 2010 ACM/IEEE International Symposium on Low-Power Electronics and Design (ISLPED)*, Austin, USA, 2010, pp. 313 - 318.

[4] D. Brunelli, C. Moser, L. Thiele, L. Benini, "Design of a solar-harvesting circuit for batteryless embedded system," IEEE Trans Circ Syst, vol. 56, no. 11, pp. 2519-2528, 2009. [Online]. Available: http://dx.doi.org/10.1109/TCSI.2009.2015690

[5] C. Park, P. H. Chou, "Ambimax: autonomous energy harvesting platform for multi-supply wireless sensor nodes," in *Proc. 3rd Annual IEEE Communications Society on Sensor and Ad Hoc Communications and Networks conference*, California, 2006, pp. 168-177. [Online]. Available: http://dx.doi.org/10.1109/SAHCN.2006.288421

[6] X. Jiang, J. Polastre, D. Culler, "Perpetual environmentally powered sensor networks," in *Proc. 4th International Symposium on Information Processing in Sensor Networks*, Los Angeles, 2005, pp.463-468. [Online]. Available: http://dx.doi.org/10.1109/IPSN.2005.1440974

[7] S. J. Chiang, H. J. Shieh, M. C. Chen, "Modeling and control of pv charger system with sepic converter," IEEE Transactions on Industrial Electronics, vol. 56, no.11, pp. 4344-4353, 2009. [Online]. Available: http://dx.doi.org/10.1109/TIE.2008.2005144

[8] K. Hoonki, M. Young-Jae, C. H. Jeong, K. Kyu-Young, K. Chulwoo, K. Soo-Won, "A 1-mW solar-energy-harvesting circuit using an adaptive mppt with a sar and a counter," IEEE Transactions on Circuits And Systems—II: Express Briefs, vol.60, no.6, pp. 331-335, 2013. [Online]. Available: http://dx.doi.org/10.1109/TCSII.2013.2258262

[9] N. Femia, G. Petrone, G. Spagnuolo, M. Vitelli, "Optimization of perturb and observe maximum power point tracking method," IEEE Trans.Power Electron., vol.20, no.4, pp.963–973, 2005. [Online]. Available: http://dx.doi.org/10.1109/TPEL.2005.850975

[10] W. Wu, N. Pongratananukul, W. Qiu, K. Rustom, T. Kasparis, I. Batarseh, "DSP-based multiple peak power tracking for expandable power system," in *Proc. 18th Annu. IEEE Appl. Power Electron. Conf. Expo.*, Florida vol.1, 2003, pp. 525–530. [Online]. Available: http://dx.doi.org/10.1109/APEC.2003.1179263

[11] M. A. Masoum, H. Dehbonei, E. F. Fuchs, "Theoretical and experimental analyses of photovoltaic systems with voltage and current-based maximum power-point tracking," IEEE Trans. Energy Convers., vol. 17, no. 4, pp. 514–522, 2002. [Online]. Available: http://dx.doi.org/10.1109/MPER.2002.4312477

[12] El. Khateb, N. A. Rahim, J. Selvaraj, M. N. Uddin, "Fuzzy logic controller based sepic converter of maximum power point tracking," in *Proc. 2012 IEEE Industry Applications Society Annual Meeting (IAS)*, Las Vegas, 2012, pp. 1-9. [Online]. Available: http://dx.doi.org/10.1109/IAS.2012.6374024

[13] L. Whei-Min, H. Chih-Ming, C. Chiung-Hsing, "Neural-network-based mppt control of a stand-alone hybrid power generation system," IEEE Trans.Power Electron., vol. 26, no.12, pp. 3571-3581, 2011. [Online]. Available: http://dx.doi.org/ 10.1109/TPEL.2011.2161775

[14] T. Esram, P. L. Chapman, "Comparison of photovoltaic array maximum power point tracking techniques," IEEE Transactions on Energy Conversion., vol. 22, no.2, pp. 439-449, 2007. [Online]. Available: http://dx.doi.org/ 10.1109/TEC.2006.874230

[15] V. Salas, A. Barrado, A. Lazaro, "Review of the maximum power point tracking algorithms for stand-alone photovoltaic systems," Solar Energy Materials & Solar Cells, vol. 90, pp. 1555-1578, 2006. [Online]. Available: http://dx.doi.org/ 10.1016/j.solmat.2005.10.023

[16] I. Houssamo, F. Locment, M. Sechilariu, "Experimental analysis of impact of mppt methods on energy efficiency for photovoltaic power systems," Int J Electr Power Energy Syst, vol. 46, pp. 98-107, 2013. [Online]. Available: http://dx.doi.org/10.1016/j.ijepes.2012.10.048

[17] M. M. Algazar, H. AL-monier, H. A. EL-halim, M. El Kotb Salem, "Maximum power point tracking using fuzzy logic control," Journal of Electrical Power and Energy Systems, vol. 39, pp. 21–28, 2012. [Online]. Available: http://dx.doi.org/ 10.1016/j.ijepes.2011.12.006

[18] Q. Mei, M. Shan, L. Liu, J. M. Guerrero, "A novel improved variable step-size incremental-resistance mppt method for pv systems," IEEE Transactions on Industrial Electronics, vol. 58, no.6, pp. 2427-2434, 2011. [Online]. Available: http://dx.doi.org/ 10.1109/TIE.2010.2064275

[19] G. Walker, "Evaluating mppt converter topologies using a matlab pv model," J. Electrical & Electronics Engineering, IEAust, vol. 21, no.1, pp. 49-56, 2001.

[20] Olivier tremblay, A. Louis Dessaint, "Experimental validation of a Battery dynamic Model for EV applications," World Electric Vehicle Journal, vol.3, pp.1-10, 2009.

[21] K. C. Wu, "Switch-mode power converters design and analysis", pp.245-247, Elsevier Academic Press, 2006.

[22] R. Ramaprabha, B. L. Mathur, "Development of an improved model of spv cell for partially shaded solar photovoltaic arrays," European Journal of Scientific Research, vol. 47, no.1, pp. 22-134, 2010.